analytical chemistry

Article

pubs.acs.org/ac

Autoenhanced Raman Spectroscopy via Plasmonic Trapping for Molecular Sensing

Soonwoo Hong,[†,‡] On Shim,[†,‡] Hyosung Kwon,[†] and Yeonho Choi*[,†,§]

[†]Department of Bio-convergence Engineering and [§]School of Biomedical Engineering, Korea University, 145, Anam-ro, Seongbuk-gu, Seoul 02841, Republic of Korea

Supporting Information

ABSTRACT: As a label-free and sensitive biosensor, surface-enhanced Raman spectroscopy (SERS) is a rapidly emerging technique. However, because SERS spectra are obtained in the area of light excitation and the enhancement effect can be varied depending on the position of a substrate, it is important to match the enhanced area with an illuminated spot. Here, in order to overcome such difficulty, we demonstrated a new technique combining SERS with plasmonic trapping. By plasmonic trapping, we can collect gold nanoparticles (GNPs) in the middle of initially fabricated nanobowtie structures where a laser is excited. As a result of trapping GNPs, hot-spots are formed at that area. Because SERS is measured in the area irradiated by a laser, hot-spot can be simultaneously coincided with a detection site for SERS. By using this, we detected Rhodamine 6G to 100 pM. To further verify and improve the reproducibility of our technique, we also calculated the electric field distribution, trapping force and trapping potential.

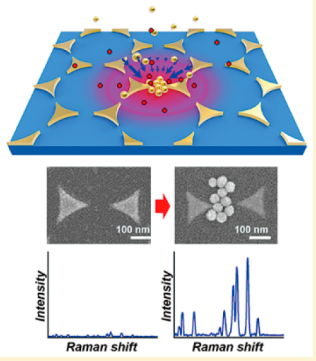

Surface-enhanced Raman spectroscopy (SERS) has been widely used to sensitively detect biomolecules since it was developed,[1,2] because it can provide the fingerprints of target molecules so that it is possible to qualitatively detect them in extremely low concentrations.[3−10] In this regard, previous SERS studies have focused on obtaining high sensitivity and selectivity by maximizing the enhancement factor,[4,6,11−18] which especially depends on which substrates researchers use for SERS.[3,10,19−21] Previously, by using focused-ion-beam lithography,[22,23] shadow overlap ion-beam lithography,[24,25] or ion-assisted aerosol lithography,[26] scientists tried to easily and efficiently fabricate substrates; however, it is still challenging to develop a more economical and time-saving method. Even though substrates are fabricated with high enhancement effect,[27,28] since it is difficult to obtain uniformly large-scaled hot spots, it needs to find hot spots and detect target molecules exactly there, which is called the "alignment" between hot spots and detection sites. Also, low reproducibility of SERS should be overcome to quantitatively detect molecules.

Here, we suggest a new technique of Raman spectroscopy using plasmonic trapping which is an advanced technique of optical trapping.[29] Plasmonic trapping is a technique that can control the position of metal structures, moving them to the desired position by the gradient of electric field intensity.[30−35] This ability to control particles to the desired position is connected to fabricating hot spots in the desired position.[36] Specifically, we can build hot spots in the desired position by trapping gold nano particles (GNPs) onto gold nano bowtie patterns which are easily fabricated by nanosphere lithography (NSL).[25,37,38] It makes gaps between nanobowtie patterns narrower, which contributes to enhancing Raman signal and trapping force because the enhancement of them depends on the electric field which is related to how narrow the structure-to-structure distances are. We can simultaneously build hot spots and obtain the signals of SERS over time by plasmonic trapping combined with conventional SERS, because the laser which is used for plasmonic trapping is also used for Raman spectroscopy at the same time. Owing to its controllability in fabricating autoenhanced areas for detection, we named the proposed technique autoenhanced Raman spectroscopy (AERS).

We initially fabricate raw nanobowtie patterns with 100 nm gap between a pair of bowties by NSL, and then decrease the gap size to less than 2 nm by attaching GNPs in between the gap using plasmonic trapping. In this manner, GNPs can be collected in the area where the laser is illuminated, and these aggregated GNPs between the gaps serve as hot spots in the SERS measurement. The proposed technique is largely based on the classical electromagnetic theory which states that either the shortened nanogaps or structures with sharp tips can strengthen the electromagnetic field which is directly connected to the enhancement of SERS signal.[39]

Through this simple method, we could clarify that hot spots could be aligned with detection sites since the GNPs were trapped at the sites where we excited by a laser, and the Raman signal was detected at that same site by the same laser. To verify effectiveness of our technique, we detected Rhodamine 6G (R6G) in various concentrations and determined that the detection limit is about 100 pM. This approach also provided quantitative data that would be difficult to obtain by

Received: April 13, 2016
Accepted: July 11, 2016

DOI: 10.1021/acs.analchem.6b01451
Anal. Chem. XXXX, XXX, XXX−XXX

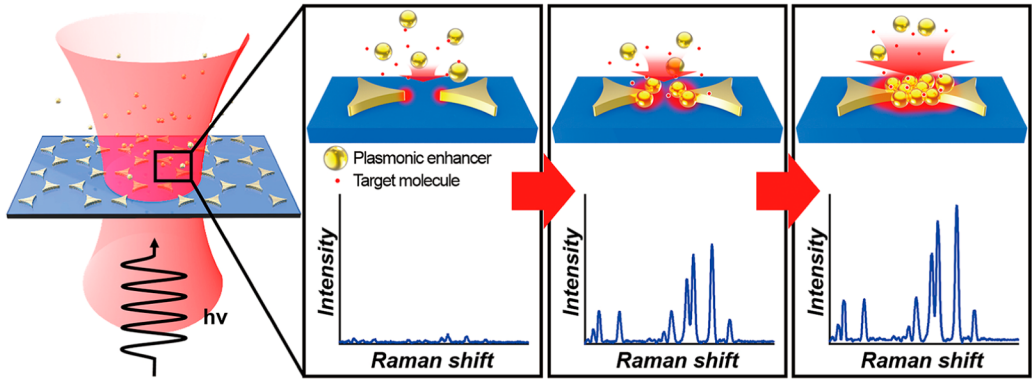

Figure 1. Schematic image of autoenhanced Raman spectroscopy (AERS). Time-dependent Raman signals were detected in 10 μM R6G solutions at 0, 120, and 240 min after laser exposure, respectively.

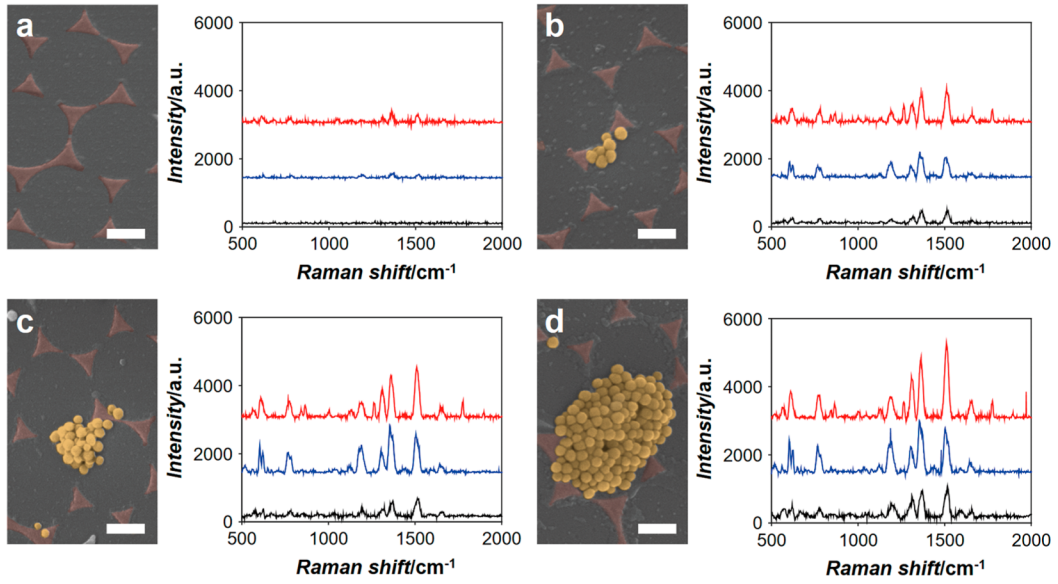

Figure 2. Time-dependent SEM images of substrate and SERS signal of R6G at (a) 0, (b) 20, (c) 40, and (d) 60 min after illumination. Each line represents different concentrations of R6G: red line means 10 μM, blue line means 1 μM, black line means 100 nM. Over time, as more GNPs are attached, structure-to-structure distances gradually decrease and AERS intensity increases. In order to clearly illustrate, nanobowties are pseudocolored as red and GNPs are done as yellow (scale bar represents 200 nm).

conventional SERS. Additionally, we tried to resolve the reproducibility problem by conducting experimental and numerical analysis. Experimentally, we conducted AERS and took scanning electron microscope (SEM) images of substrate morphology over time. Numerically, we calculated the electric field distribution, which is contributed to the enhancement of the signal, and trapping force and trapping potential, which are contributed to understanding plasmonic trapping.

EXPERIMENTAL SECTION

The fabrication method involves patterning 500 nm polystyrene (PS) beads on a cover glass by drop casting. Initially, the cover glass is washed thoroughly with piranha solution to make the surface more hydrophilic and clearer, where the ratio of H_2O_2 to H_2SO_4 is 1:3. After cleansing, to form a monolayer of PS beads, we drop 15 μL of solution of 500 nm PS beads (Polyscience, U.S.A.). Then gold is deposited onto a previously fabricated monolayer of PS beads to a thickness of 30 nm using an e-gun evaporator (ZZS550−2/D, Maestech, Republic of Korea). The remained PS beads are removed using a plastic tape and toluene solution. As a result, raw nanobowtie patterns can be obtained. These patterns are made of hexagonal arrays with an approximately 100 nm structure-to-structure distances. The SEM image of raw nanobowtie is shown in Supporting Information.

We set a polydimethylsiloxane (PDMS; Dow Corning, U.S.A.) well on the arrays and load the mixture of analytes for SERS, in which the mixture consists of 100 μL of R6G (Sigma-Aldrich, U.S.A.) and 100 μL of a colloidal solution of 50 nm GNPs (BBI Solutions, U.K.). Then we cover the top of the well with a cover glass to prevent evaporation during the AERS process and set the substrate on a microscope (Carl Zeiss Axiovert 200 inverted microscope, Germany). A 785 nm wavelength laser (CNI MDL-III-785 nm, China) is focused on the substrate. After the GNPs are attached, the enhanced signal can be observed at the same time when the substrate is being formed. We used 10 mW laser and set acquisition time to 10 s.

Finite-element method (FEM) simulations are performed by using COMSOL Multiphysics (COMSOL Inc., Sweden). A single geometric nanobowtie is fabricated by three cylinders (r = 500 nm, h = 30 nm), and for practicality, we use a filet function to make a curved edge. The radii of the curvature are

DOI: 10.1021/acs.analchem.6b01451
Anal. Chem. XXXX, XXX, XXX−XXX

500, 9, or 6 nm. The detailed geometry is shown in Figure S3. In the model, a pair of single nanobowties are located on a glass, leaving a space of 100 nm. Water is used as the medium above the substrate. A 785 nm laser is illuminated on the geometry from the bottom, which is *x*-polarized, the power of the light is 6.802 GW/m^2 and the E_0 of the light is 1.963 MV/m. All of the parameters reflect the experimental setup. As a boundary condition, we use perfectly matched layers (PMLs) that cover the entire geometry like a thin crust; the PMLs are colored as blue in Figure S4. These PMLs absorb all of the incident light and make it possible for us to focus on the region of interest, particularly the nanobowtie and GNPs. All the simulations are run on a Dell Precision T7600 with Xeon CPU E5−2630 2.30 GHz (6 processors) and 128 GB of memory and the minimum mesh size is less than 1 nm.

RESULTS AND DISCUSSION

Figure 1 schematically shows the process of detecting R6G by AERS. Initially, we fabricate gold nanobowtie patterns by NSL. Then, after loading a mixture of GNPs and R6G on nanobowtie patterns, we illuminate a laser into the substrate, in which the calculated laser spot size is approximately 1.470 μm^2. Over time, GNPs are attached to the sharp tips of initially formed nanobowties by plasmonic trapping and it gradually decreases the gap size between bowties and it increases Raman intensity. As an initial substrate, nanobowtie patterns significantly work as a prime antenna. Without any bowtie patterns in the initial step, the trapping forces exerted on GNPs are not enough to trap GNPs, ultimately causing GNPs to be randomly distributed on the substrate.

The narrow gaps fabricated by plasmonic trapping generate a strong electromagnetic field, and the enhanced electromagnetic field contributes to enhancing Raman signal, simultaneously. Interestingly, we need only one laser in order to attract GNPs to the focused area by plasmonic trapping and strengthen Raman signal at the same area over time. In other words, it is possible to detect Raman signals of biomolecules by exposing plasmonic enhancers, or GNPs and target molecules, or R6G, on basic nanobowties by a single laser.

Experimentally, we obtained SEM images of each structure and AERS signal of R6G by using our technique over time as seen in Figure 2. Figure 2a−d represent SEM images and AERS signals at 0, 20, 40, and 60 min after laser illumination, respectively. GNPs are attracted to the desired sites where we illuminate by a laser. This means that we can control the position of hot spots and can also detect target molecules there at the same time. In Figure 2, each color line represents different concentrations of R6G; red line represents 10 μM, blue line represents 1 μM and black line represents 100 nM. These R6G in low concentrations cannot be detected only by raw bowties; however, as time goes by, the intensity of signals gradually increases. This is because additionally attached GNPs can enhance the electric field and trapping force enough to trap more and more GNPs as they shorten the structure-to-structure distances. With 15 mW laser, we could detect R6G to the concentration of 100 pM and the data are represented in Figure S6.

Our concept has differences with conventional SERS using nanogaps of randomly aggregated GNPs. They depend on whether many GNPs are intensively aggregated at specific spots because it is uncontrollable to collect GNPs together. Even after they are well aggregated, researchers should find the hot-spots with highly shorten nano gaps and detect the Raman signals at that position, but it is impracticable to find nano structures by a microscope during experiments. However, since we use plasmonic trapping, we can control aggregation sites, or hot-spots and also simultaneously detect target molecules at exactly same sites. Unlike conventional SERS, in which the data can vary by a lot of variables, our method reduces these variables due to high controllability, which is directly contributed to increasing reproducibility.

Also, we quantitatively analyzed the AERS of R6G as shown in Figure 3. Figure 3a shows the AERS signals of 100 nM R6g

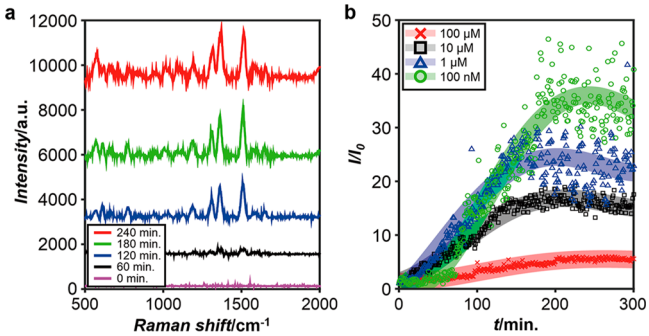

Figure 3. Quantitative analysis for R6G by AERS. (a) AERS signals of 100 nM R6G after 0 to 240 min. (b) Time-dependent relative AERS intensities of R6G against the initial intensities of R6G at 1510 cm^{-1}.

after 0 to 240 min after laser illuminates, in which the signal at 0 min signifies AERS on raw bowtie patterns and the signal at 240 min signifies that on the completed AERS substrate. A nearly flat signal at 0 min increases by 40 fold after 240 min by construction of a completed AERS substrate. In Figure 3b, we tried to show how much the enhancement increased in case of each concentration. In this regard, we used I/I_0 as *y* axis to illustrate how much the signal at each time, I, is enhanced compared to the initial signal, I_0. What is intriguing is that the trend of increment is clearer in case of low concentrations such as 100 nM rather than in relatively high concentrations. This is because R6G in lower concentration initially has extremely weak SERS signals so that the value of I_0, or the denominator, becomes smaller. So, if the intensity is strengthened as gap size decreases over time, the value can become relatively bigger. By the same reason, because the Raman signals of target molecules in a relatively dense solution can be detected on raw nanobowties, it seems as though they are not fully enhanced.

We numerically analyzed AERS with a FEM tool, as well. These numerical simulations can support our experiment results as a proof. Also, we tried to verify that the electric field is enough to effectively enhance SERS signal and trapping force is strong enough to attract GNPs into the desired position. So, we first calculated the electric field distribution surrounding our substrate, which is related to the enhancement of SERS signals. It is known that the intensity of SERS signal is proportional to the fourth power of electric field. Particularly on a focal plane, the enhancement of electric field has maximum value. So, we simplified structures for numerical analysis equal to the experimental structures only on the focal planes, where we set a focal plane as 25 nm by *z*-axis. As seen in Figure 4a−c, it is recognizable that the schematic images for simulation are equal to the experimental structures at 0, 20, and 40 min after illumination, respectively.

Figure 4d−f shows the numerical results of electric field distribution in case of different structures which are represented

DOI: 10.1021/acs.analchem.6b01451
Anal. Chem. XXXX, XXX, XXX−XXX

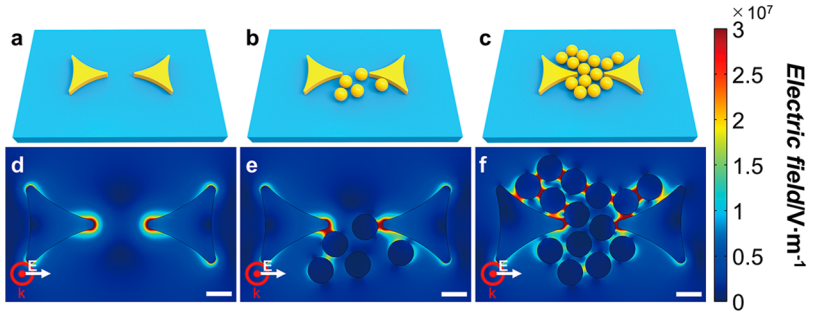

Figure 4. Electric field distribution over time: (a–c) schematic images of structures for numerical analysis; (d–f) electric distribution on the focal plane. As more particles are attached over time, not only does the maximum value of electric field increase, but also the area of hot spots becomes broadened.

in Figure 4a–c, respectively. In Figure 4d, at the beginning, there is no strong electric field and limited hot spot area. However, as time goes by, as more particles are attached in between the gap by plasmonic trapping, the substrate has decreased the structure-to-structure distances, and it is connected to increasing electric field and broadening hot spot. In Figure 4e, the structure at 20 min after illumination has more powerful gradient of electric field and has broader hot spots area compared to the initial raw bowtie. A total of 20 min after then, the enhancement is extremely strengthened and the area of hot spots highly increases, as represented in Figure 4f. Compared with the maximum value of electric field in case of Figure 4d, that in case of Figure 4f is more than 4-fold.

We previously mentioned that plasmonic trapping is one of the significant factors in our research; thus, it is necessary to obtain the trapping force for plasmonic trapping. The force of plasmonic trapping is typically proportional to the square of the electric field gradient. In this regard, gradually shortening gap over time generates the enhanced trapping force in which the trend of increment is equal to the electric field distribution in Figure 4. That is, as GNPs are attached between bowties and they are closely packed, the enhanced trapping force sequentially generates stronger attraction. Thus, to further verify AERS, we performed numerical analyses of trapping force and trapping potential in addition to calculating the electric field distribution.

Figure 5 includes trapping force and potential calculation. Initially, we calculated trapping forces in case that a GNP is attached to the base by 10 nm from a bowtie. By conventional electromagnetic theory, it could be calculated. According to other researches about optical or plasmonic trapping, the trapping force is expressed as[40,41]

$$F = \oint_s (T \cdot n) ds \tag{1}$$

, where T represents Maxwell stress tensor and n is the normal vector perpendicular to the surface. Trapping force can be also derived from polarizability, but because T and n are easily calculated by COMSOL, we used this equation. A floating GNP, represented as a gold dashed circle in Figure 5a, is freely moving around the fabricated gap such that it would be attracted by the trapping force. Its magnitude greatly increases around the gap, where the electric field highly strengthened. Thus, the trapping force reaches nearly 4 pN at 55 nm by z-axis. In addition, as mentioned, the gap size decreases with GNPs attached and it sequentially causes the trapping force to be enhanced. In Figure 5a, the reason why the direction of trapping force seems toward the surface of nanobowtie, not the gap of nanobowtie is that we assumed that the simulation condition has under 10 nm gap. In other words, since 50 nm

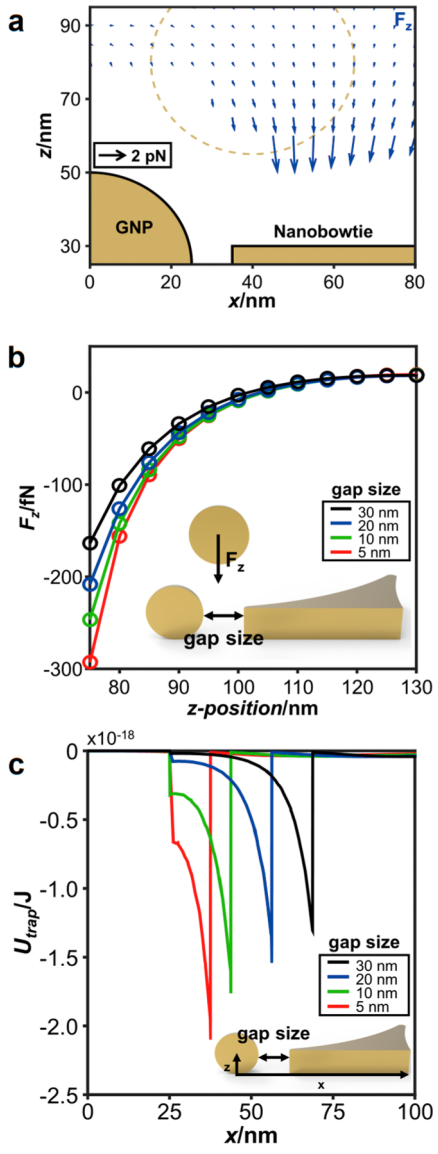

Figure 5. Numerical analysis for trapping force and trapping potential. (a) Calculated trapping force exerted on a floating GNP in vector expression, where the floating GNP is represented by gold dash line, in case that the gap size between attached GNP and nanobowtie is 10 nm (blue arrows represent F_z). (b) Trapping force and (c) trapping potential were calculated by the gap sizes, as well.

DOI: 10.1021/acs.analchem.6b01451
Anal. Chem. XXXX, XXX, XXX–XXX

GNP cannot be moved in between 10 nm gap, the numerical results are shown like that. Specifically, this is because we fixed the attached GNP in the bottom of substrate so that the floating GNP cannot push the already trapped particle. We simplified the structure and physics of simulation by using steady-state model and tried to explain that the trapping force is enough to trap GNPs at each time or by each gap size.

To further numerically verify our idea that attached GNPs decrease gap size and it sequentially strengthens both the trapping force and AERS signals, we calculated the trapping force and trapping potential by gap sizes. As represented in Figure 5b,c, the trapping force and trapping potential precisely match the experimental data. In Figure 5b, as particles are attached near the gap, which increasingly decreases structure-to-structure distances in raw bowties, the trapping force exerted on a GNP at 75 nm by z-axis reaches approximately 300 fN in case of a 5 nm gap size. This value is enough to effectively trap GNP to the illuminated spot compared to other plasmonic trapping researches;[31,41] however, we also tried to exactly calculate trapping potential in order to clarify whether our plasmonic trapping can excel other forces, especially Brownian motion. Trapping potential, U_{trap}, is given by[31,40,42]

$$U_{trap} \approx -\int F dr = -\frac{\alpha'}{2}\langle E^2 \rangle \tag{2}$$

$$\alpha = \alpha' + i\alpha'' = 3V\frac{\varepsilon_p - \varepsilon_m}{\varepsilon_p + 2\varepsilon_m} \tag{3}$$

, where $\langle E^2 \rangle$ means the time-averaged square of the electric field, α represents polarizability of the trapped particle, V is the volume of the particle, and ε_p and ε_m are the permittivity of particle and the surrounding medium, respectively. As seen in Figure 5c, the narrower gap size decreases, the more trapping potential occurs. The depth of the potential well reaches ~2.2 $\times 10^{-18}$J, about three orders of value larger than the kinetic energy of Brownian motion. At room temperature, it can be calculated by the equation $k_BT = 4 \times 10^{-21}$ J, where k_B is Boltzmann's constant. This means that plasmonic trapping by using nanobowtie arrays can theoretically attract GNPs in between gaps. Compared to other plasmonic trapping researches, the calculated optical potential seems too exaggerated, but this is because we used 10 mW laser and tried to trap 50 nm GNPs since the trapping potential is proportional to the square of electric field intensity and inversely proportional to the cube of radius of trapping particles, as seen in the eq 3. It can be predicted to generate more highly enhanced trapping force in the case of gap size of less than 1 nm, which could not be achieved because of computing limitations.

CONCLUSIONS

We introduced AERS as a new Raman spectroscopy technique and verified it by using experimental and numerical analyses. Our technique by combining plasmonic trapping with conventional SERS could successfully detect R6G to 100 pM and quantitatively obtain Raman signals. A numerical analysis based on the FEM method showed that AERS corresponds well with the experimental data, which also helps to explain the mechanism of AERS. In this regard, we did not only simplify the fabrication method, but we could also overcome the difficulties of aligning hot spots with the detection sites and increase reproducibility. In the future, we envision that a variety of biomolecules will be specifically detected by our technology as a preprocessing-free biosensor, and our technology could be developed as a lab-on-a-chip by combining it with microfluidics.

ASSOCIATED CONTENT

Supporting Information

The Supporting Information is available free of charge on the ACS Publications website at DOI: 10.1021/acs.analchem.6b01451.

Schematic diagrams of fabrication procedure; SEM images of raw nano bowtie pattern; geometry used in the simulation; governing equations; SEM images of trapped GNPs; time-dependent data in case of 15 mW laser power (PDF).

AUTHOR INFORMATION

Corresponding Author

*E-mail: yeonhochoi@korea.ac.kr. Tel.: +82-2-3290-5657.

Author Contributions

‡These authors contributed equally (S.H. and O.S.).

Notes

The authors declare no competing financial interest.

ACKNOWLEDGMENTS

This research was supported by a grant of the Korea Health Technology R&D Project through the Korea Health Industry Development Institute (KHIDI), funded by the Ministry of Health & Welfare, Republic of Korea (Grant Nos.: HI14C2537 and HR14C0007).

REFERENCES

(1) Nie, S.; Emory, S. R. *Science* **1997**, *275*, 1102−1106.
(2) Kneipp, K.; Wang, Y.; Kneipp, H.; Perelman, L. T.; Itzkan, I.; Dasari, R. R.; Feld, M. S. *Phys. Rev. Lett.* **1997**, *78*, 1667−1670.
(3) Camden, J. P.; Dieringer, J. A.; Zhao, J.; Van Duyne, R. P. *Acc. Chem. Res.* **2008**, *41*, 1653−1661.
(4) Hatab, N. A.; Hsueh, C.-H.; Gaddis, A. L.; Retterer, S. T.; Li, J.-H.; Eres, G.; Zhang, Z.; Gu, B. *Nano Lett.* **2010**, *10*, 4952−4955.
(5) Kang, J. W.; So, P. T.; Dasari, R. R.; Lim, D.-K. *Nano Lett.* **2015**, *15*, 1766−1772.
(6) Kleinman, S. L.; Sharma, B.; Blaber, M. G.; Henry, A.-I.; Valley, N.; Freeman, R. G.; Natan, M. J.; Schatz, G. C.; Van Duyne, R. P. *J. Am. Chem. Soc.* **2013**, *135*, 301−308.
(7) Kumar, G. P. *J. Nanophotonics* **2012**, *6*, 06450301−06450320.
(8) Li, J. F.; Huang, Y. F.; Ding, Y.; Yang, Z. L.; Li, S. B.; Zhou, X. S.; Fan, F. R.; Zhang, W.; Zhou, Z. Y.; Ren, B. *Nature* **2010**, *464*, 392−395.
(9) Lim, D.-K.; Jeon, K.-S.; Hwang, J.-H.; Kim, H.; Kwon, S.; Suh, Y. D.; Nam, J.-M. *Nat. Nanotechnol.* **2011**, *6*, 452−460.
(10) Theiss, J.; Pavaskar, P.; Echternach, P. M.; Muller, R. E.; Cronin, S. B. *Nano Lett.* **2010**, *10*, 2749−2754.
(11) Alu, A.; Engheta, N. *Nat. Photonics* **2008**, *2*, 307−310.
(12) Becker, J.; Zins, I.; Jakab, A.; Khalavka, Y.; Schubert, O.; Sönnichsen, C. *Nano Lett.* **2008**, *8*, 1719−1723.
(13) Flauraud, V.; Van Zanten, T. S.; Mivelle, M.; Manzo, C.; Garcia-Parajo, M.; Brugger, J. *Nano Lett.* **2015**, *15*, 4176−4182.
(14) Liu, N.; Tang, M. L.; Hentschel, M.; Giessen, H.; Alivisatos, A. P. *Nat. Mater.* **2011**, *10*, 631−636.
(15) Ropers, C.; Neacsu, C.; Elsaesser, T.; Albrecht, M.; Raschke, M.; Lienau, C. *Nano Lett.* **2007**, *7*, 2784−2788.
(16) Schuller, J. A.; Barnard, E. S.; Cai, W.; Jun, Y. C.; White, J. S.; Brongersma, M. L. *Nat. Mater.* **2010**, *9*, 193−204.
(17) Stockman, M. I. *Phys. Rev. Lett.* **2004**, *93*, 137404.
(18) Su, K.-H.; Wei, Q.-H.; Zhang, X.; Mock, J.; Smith, D. R.; Schultz, S. *Nano Lett.* **2003**, *3*, 1087−1090.

DOI: 10.1021/acs.analchem.6b01451
Anal. Chem. XXXX, XXX, XXX−XXX

(19) Hong, S.; Kang, T.; Choi, D.; Choi, Y.; Lee, L. P. *ACS Nano* **2012**, *6*, 5803−5808.
(20) Jeong, E.; Kim, K.; Choi, I.; Jeong, S.; Park, Y.; Lee, H.; Kim, S. H.; Lee, L. P.; Choi, Y.; Kang, T. *Nano Lett.* **2012**, *12*, 2436−2440.
(21) Ou, F. S.; Hu, M.; Naumov, I.; Kim, A.; Wu, W.; Bratkovsky, A. M.; Li, X.; Williams, R. S.; Li, Z. *Nano Lett.* **2011**, *11*, 2538−2542.
(22) Fan, M.; Andrade, G. F.; Brolo, A. G. *Anal. Chim. Acta* **2011**, *693*, 7−25.
(23) Tong, H. D.; Jansen, H. V.; Gadgil, V. J.; Bostan, C. G.; Berenschot, E.; van Rijn, C. J.; Elwenspoek, M. *Nano Lett.* **2004**, *4*, 283−287.
(24) Choi, Y.; Hong, S.; Lee, L. P. *Nano Lett.* **2009**, *9*, 3726−3731.
(25) Kosiorek, A.; Kandulski, W.; Chudzinski, P.; Kempa, K.; Giersig, M. *Nano Lett.* **2004**, *4*, 1359−1363.
(26) Jung, K.; Hahn, J.; In, S.; Bae, Y.; Lee, H.; Pikhitsa, P. V.; Ahn, K.; Ha, K.; Lee, J. K.; Park, N. *Adv. Mater.* **2014**, *26*, 5924−5929.
(27) Liu, Z.; Yang, Z.; Peng, B.; Cao, C.; Zhang, C.; You, H.; Xiong, Q.; Li, Z.; Fang, J. *Adv. Mater.* **2014**, *26*, 2431−2439.
(28) Oh, Y. J.; Jeong, K. H. *Adv. Mater.* **2012**, *24*, 2234−2237.
(29) Maragò, O. M.; Jones, P. H.; Gucciardi, P. G.; Volpe, G.; Ferrari, A. C. *Nat. Nanotechnol.* **2013**, *8*, 807−819.
(30) Erickson, D.; Serey, X.; Chen, Y.-F.; Mandal, S. *Lab Chip* **2011**, *11*, 995−1009.
(31) Juan, M. L.; Righini, M.; Quidant, R. *Nat. Photonics* **2011**, *5*, 349−356.
(32) Min, C.; Shen, Z.; Shen, J.; Zhang, Y.; Fang, H.; Yuan, G.; Du, L.; Zhu, S.; Lei, T.; Yuan, X. *Nat. Commun.* **2013**, *4*, 2891.
(33) Roxworthy, B. J.; Ko, K. D.; Kumar, A.; Fung, K. H.; Chow, E. K.; Liu, G. L.; Fang, N. X.; Toussaint, K. C., Jr *Nano Lett.* **2012**, *12*, 796−801.
(34) Urban, A. S.; Carretero-Palacios, S.; Lutich, A. A.; Lohmüller, T.; Feldmann, J.; Jäckel, F. *Nanoscale* **2014**, *6*, 4458−4474.
(35) Wang, K.; Crozier, K. B. *ChemPhysChem* **2012**, *13*, 2639−2648.
(36) Wang, K.; Schonbrun, E.; Steinvurzel, P.; Crozier, K. B. *Nat. Commun.* **2011**, *2*, 469.
(37) Cheung, C. L.; Nikolić, R.; Reinhardt, C.; Wang, T. *Nanotechnology* **2006**, *17*, 1339−1343.
(38) Peng, K.; Zhang, M.; Lu, A.; Wong, N.-B.; Zhang, R.; Lee, S.-T. *Appl. Phys. Lett.* **2007**, *90*, 163123.
(39) Brown, L. V.; Yang, X.; Zhao, K.; Zheng, B. Y.; Nordlander, P.; Halas, N. J. *Nano Lett.* **2015**, *15*, 1272−1280.
(40) Shoji, T.; Tsuboi, Y. *J. Phys. Chem. Lett.* **2014**, *5*, 2957−2967.
(41) Zhang, W.; Huang, L.; Santschi, C.; Martin, O.J. F. *Nano Lett.* **2010**, *10*, 1006−1011.
(42) Novotny, L.; Hecht, B. *Principles of Nano-Optics*, 2nd ed.; Cambridge University Press, 2012.

DOI: 10.1021/acs.analchem.6b01451
Anal. Chem. XXXX, XXX, XXX−XXX